Progress In Electromagnetics Research, *PIER 28, 275–294, 2000*

MICROWAVE IMAGING OF PARALLEL PERFECTLY CONDUCTING CYLINDERS USING REAL-CODED GENETIC ALGORITHM COUPLED WITH NEWTON-KANTORIVITCH METHOD

A. Qing and C. K. Lee

School of Electrical and Electronic Engineering
Nanyang Technological University
Nanyang Avenue
Singapore 639798

1. INTRODUCTION

The electromagnetic inverse scattering problem [l–4] is to recover information concerning some inaccessible region from the scattered electromagnetic fields measured outside. It has been one of the most challenging research topics in recent years due to its considerable practical importance in various areas of technology [1–14] such as non-destructive evaluation, subsurface and ground-penetrating radar, geophysical remote sensing, medical imaging, seismology and target identification etc. However, it is difficult to solve because of its ill-posedness and nonlinearity [1–4, 15–17]. It is the multiple scattering effects that make the electromagnetic inverse scattering problem inherently nonlinear while contaminated and insufficient measuring data result in the ill-posedness.

Much attention has been paid to developing the inversion algorithms and a variety of algorithms have been proposed. Generally, they fall into two classes, namely the analytic solution and the numerical solution.

Most of the analytic inversion algorithms [18–25] deal with one dimension problem. They usually make use of some approximations such as the physical optics approximation [19–20], the Born and Rytov approximation [21, 26], etc., to simplify the problem. These inversion algorithms include the layer-stripping algorithm [2, 14], the method of characteristics [2, 14, 22], the Gel'fand-Levitan integral equation method [23] and the Marchenko integral equation method [23–25], etc. However, we hardly encounter situations where a one-dimensional model can practically be used. Moreover, the simplicity of these algorithms in one dimension is not preserved in higher dimension. Consequently, they have only theoretical significance but limited practical applications.

In contrast, the numerical inversion algorithms [27–52] solve the electromagnetic inverse problem numerically and iteratively. They can deal with not only one-dimensional but higher dimensional problems.

The electromagnetic inverse problem can be transferred into an optimization problem. Correspondingly, the numerical inversion algorithms can be further classified into two categories according to the optimization algorithms adopted. The first is the local inversion algorithm and the second is the global inversion algorithm.

Most of the previous numerical inversion algorithm belong to the first category. The prominent algorithms of this category include the Born iterative method (BIM) [27, 28], the distorted Born iterative method (DBIM) [29, 30], the Newton-Kantorivitch method (NKM) [31–33], the Leven-berg-Marquardt algorithm [34–36], local shape function (LSF) method [37–40], the modified gradient method (MGM) [41–43], the pseudoinverse transformation method [44], the dual space method [4] and the nonlinear parameter optimization method [45, 46], etc.

The above mentioned local inversion algorithms are gradient based. They are restricted to relatively small gradients of the object functions since the optimization methods adopted in them are local. Thus, they only converge to the true profile under certain conditions, otherwise, they may be trapped into a local extreme or even diverge. For example, the BIM and DBIM can only give convergent solutions when the scatterer is weak while the Newton-Kantorivitch method demands a good starting point. A *priori* is crucial. Unfortunately, such a *priori* knowledge is not always available or accurate enough.

More recently, a new class of inverse scattering algorithms has emerged. They are the global inversion algorithms [47–52] based on genetic algorithms (GAs) [53–56]. GAs are a set of slowly converging probabilistic global optimization methods based on genetic recombination and evolution in nature. They operate on a randomly generated population in the search space simultaneously and perform a global optimization by the three genetic operations, i.e., selection, crossover and mutation. The GAs are less prone to converge to a local optimum than the gradient based algorithms even when the initial guess is far away from the exact one because they are stochastic and global in nature. GAs have been widely used in solving electromagnetic problems [57–61]. However, its application in solving electromagnetic inverse problem is new and incomplete.

Chiu and Liu [47] tried to reconstruct the image of a perfectly conducting cylinder by the standard genetic algorithm (SGA). However, the reported results are dubious [48, 49]. Qing and Lee [48] dealt with the same problem by RGA. RGA was also used to solve the microwave imaging problem of multiple perfectly conducting cylinders [49, 50]. Xiao et al. [51] solved the same problem by micro genetic algorithm (MGA) coupled with Powell method, while Meng et al. [52] dealt with it by SGA incorporated with local shape function (LSF) method.

The GA-based global inversion algorithms offer many advantages over the local inversion algorithms such as strong search ability, simplicity, versatility, high level of robustness and insensitiveness to ill-posedness. However, they also exhibit several disadvantages among which the unendurable long inversion time is the most notorious.

In this paper, a novel method, the RGA-NKM, is proposed for microwave imaging of parallel perfectly conducting cylinders with or without the effect of random noise. It is developed to reduce the untolerably long inversion time of RGA while keeping the merits of RGA. The main idea of the RGA-NKM is to perform a Newton-Kantorivitch type search for the local optimum after the genetic operations in each genetic evolution to improve the local search ability of RGA. It begins from an initial population which is generated randomly within the search space. Then, the algorithm enters into evolution loop searching for the optimum solution. The evolution continues until the termination conditions are fulfilled. Numerical results and comparisons with both RGA and NKM demonstrate that although the simplicity of RGA is lost, the search ability is greatly improved and the convergence is sped up significantly while those merits of RGA such as high level of robustness, versatility and insensitiveness to ill-posedness are retained.

2. FORMULATION OF PROBLEM

The problem considered here is the same as that in [49] which is depicted in Fig. 1. R stands for receivers located on the measuring circle Ω with radius R^{meas}. O is the origin. C_1 and C_2 are the contours of the two perfectly conducting cylinders. O_i is the local origin of C_i which is an arbitrary point inside C_i. $|OO_i| = d_i$. C_1 and C_2 are denoted by the shape functions $F_1(\theta)$ and $F_2(\theta)$ respectively. The shape functions are assumed to be trigonometric series of order $N/2$

$$F_i(\theta) = \sum_{n=0}^{N/2} A_{in}\cos(n\theta) + \sum_{n=1}^{N/2} B_{in}\sin(n\theta) \qquad i = 1, 2 \tag{1}$$

The two cylinders are assumed to be illuminated by TM plane wave with time harmonic factor $e^{j\omega t}$

$$\mathbf{E}^{inc}(\mathbf{r}) = E^{inc}(\mathbf{r})\hat{z} = e^{-jk_0(x\cos\varphi + y\sin\varphi)}\hat{z} \tag{2}$$

where $\omega = 2\pi f$ is the angular frequency, $\mathbf{r} = (x, y)$, φ is the incident angle and $\hat{z}$ is the unit vector in the z direction.

Surface currents $\mathbf{J}_{sj}(\mathbf{r}) = J_{sj}(\mathbf{r})\hat{z}$, $j = 1, 2$ are induced on the surface of the cylinders and the scattered electric field $\mathbf{E}^{scat}(\mathbf{r}) = E^{scat}(\mathbf{r})\hat{z}$ is subsequently generated

$$\begin{aligned} E^{scat}(\mathbf{r}) &= \sum_{j=1}^{2} -\frac{\omega\mu_0}{4}\int_{C_j} J_{sj}(\mathbf{r}')H_0^{(2)}(k_0|\mathbf{r}-\mathbf{r}'|)d\mathbf{r}' \\ &= \sum_{j=1}^{2} -\frac{\omega\mu_0}{4}\int_0^{2\pi} J_j(\theta')H_0^{(2)}(k_0|\mathbf{r}-\mathbf{r}'|)d\theta' \end{aligned} \tag{3}$$

where $H_0^{(2)}(\cdot)$ is the second kind Hankel's function of zero order, k_0 is the wavenumber of free space

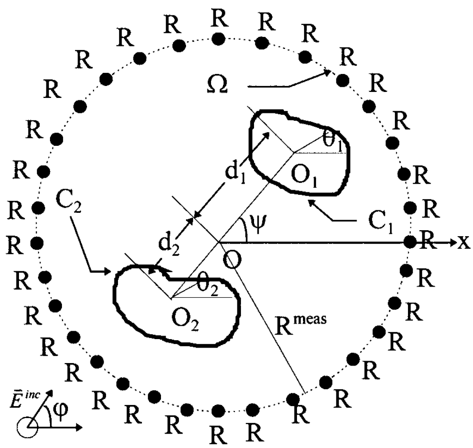

Figure 1. Geometry of problem in this paper.

$$J_j(\theta') = \sqrt{F_j^2(\theta') + F_j'^2(\theta')} \cdot J_{sj}(\mathbf{r}')\Big|_{\mathbf{r}'=[F_j(\theta')\cos\theta' \pm d_j\cos\psi, F_j(\theta')\sin\theta' \pm d_j\sin\psi]}$$

where the $+$ sign is to be employed for $j = 1$ and the $-$ sign for $j = 2$.

At the surface of each cylinder, the electric field satisfies the boundary condition

$$\left[\mathbf{E}^{scat}(\mathbf{r}) + \mathbf{E}^{inc}(\mathbf{r})\right] \cdot \hat{z} = 0 \qquad \mathbf{r} \in C_i \tag{4}$$

Thus

$$E^{inc}(\mathbf{r}) = \sum_{j=1}^{2} \frac{\omega\mu_0}{4} \int_0^{2\pi} J_j(\theta') H_0^{(2)}(k_0 R_{ij}) d\theta' \tag{5}$$

where

$$R_{ij} = \left|\mathbf{r} - \mathbf{r}'\right| \qquad \mathbf{r} \in C_i,\ \mathbf{r}' \in C_j$$

The distribution of surface current is obtained after solving Eq. (5) by point-matching method [62] with pulse basis function and Dirac delta test function. Consequently, the scattered electric field at receivers on Ω is

$$E^{scat}(\mathbf{r}) = \sum_{j=1}^{2} -\frac{\omega\mu_0}{4} \int_0^{2\pi} J_j(\theta') H_0^{(2)}(k_0 R_j) d\theta' \tag{6}$$

where

$$R_j = \left|\mathbf{r} - \mathbf{r}'\right| \qquad \mathbf{r} \in \Omega,\ \mathbf{r}' \in C_j$$

For the inverse problem, the scattered electric field $\mathbf{E}^{scat}_{meas}$, at receivers on Ω are measured and known while the shape functions, i.e., the coefficients of the trigonometric series are unknown.

A relative error function with respect to the coefficients of the trigonometric series is defined as

$$f^n(\mathbf{x}) = \left\|\mathbf{E}^{scat}_{meas} - \mathbf{E}^{scat}_{n}\right\| / \left\|\mathbf{E}^{scat}_{meas}\right\| \tag{7}$$

where

$$\mathbf{x} = \begin{bmatrix} A_{10} & A_{11} & \cdots & A_{1N/2} & B_{11} & B_{12} & \cdots & B_{1N/2} \\ A_{20} & A_{21} & \cdots & A_{2N/2} & B_{21} & B_{22} & \cdots & B_{2N/2} \end{bmatrix}$$

$$\left\|\mathbf{E}^{scat}_{meas}\right\| = \sqrt{\sum_{j=1}^{N_f \times N_a \times N_r} \left[\left(E^{scat}_{meas}\right)_j\right]^2},$$

$$\left\|\mathbf{E}^{scat}_{meas} - \mathbf{E}^{scat}_{n}\right\| = \sqrt{\sum_{j=1}^{N_f \times N_a \times N_r} \left[\left(E^{scat}_{meas}\right)_j - \left(E^{scat}_{n}\right)_j\right]^2}$$

$\mathbf{E}^{scat}_{meas}$ and $\mathbf{E}^{scat}_{n}$ are $N_f \times N_a \times N_r$-dimensional vectors containing the scattered electric field measured and computed after n iterations respectively. N_f, N_a, and N_r are the total number of frequencies, incident angles and receivers respectively.

The relative error function gives a measurement on how close the inverted results approaches the true profile.

The inverse problem can therefore be cast into an optimization problem by minimizing the relative error function with the coefficients of the trigonometric series being the parameters to be optimized.

3. REAL-CODED GENETIC ALGORITHM

The real-coded genetic algorithm has been successfully applied to solve the above inverse problem [49]. For this case, the i-th creature among the nth population takes the form

$$\mathbf{x}^{n,i} = \begin{bmatrix} A^{n,i}_{10} & A^{n,i}_{11} & \cdots & A^{n,i}_{1N/2} & B^{n,i}_{11} & B^{n,i}_{12} & \cdots & B^{n,i}_{1N/2} \\ A^{n,i}_{20} & A^{n,i}_{21} & \cdots & A^{n,i}_{2N/2} & B^{n,i}_{21} & B^{n,i}_{22} & \cdots & B^{n,i}_{2N/2} \end{bmatrix} \tag{8}$$

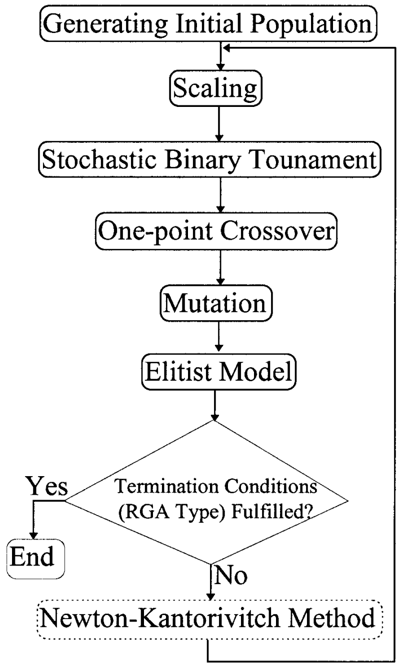

Figure 2. Flow chart of RGA-NKM/RGA for microwave imaging of two parallel perfectly conducting cylinders.

The corresponding object functions is

$$f^n(\mathbf{x}^{n,i}) = \left\| \mathbf{E}_{meas}^{scat} - \mathbf{E}_{n,i}^{scat} \right\| / \left\| \mathbf{E}_{meas}^{scat} \right\| \tag{9}$$

where $\mathbf{E}_{n,i}^{scat}$ is a $N_f \times N_a \times N_r$-dimensional vector containing the computed scattered electric field corresponding to $\mathbf{x}^{n,i}$.

The RGA begins from an initial population of size N_{pop} which are generated randomly within the search space. Then, the population enters the main GA loop for searching the optimum solution of the problem. Scaling, stochastic binary tournament selection, one-point crossover and mutation are involved in a GA loop. The GA loop continues until the termination conditions are fulfilled. The termination conditions for the RGA are:

(1) $\min f^n(\mathbf{x}^{n,i}) < \varepsilon$, where ε is the required accuracy
(2) Maximum evolutions are used up
(3) The RGA is trapped into local minima

The flow chart of RGA for microwave imaging of two parallel perfectly conducting cylinders is depicted in Fig. 2 where the block in dotted diagram should not be included for this case.

It has been demonstrated in [49] that the RGA performs well with respect to search ability, versatility, insensitiveness to ill-posedness, robustness and simplicity. The probabilistic nature of the RGA allows random starting and requires almost no initial guesses. A false assumption on the values of d_1, d_2 and Ψ is also acceptable. However, the inversion time is untolerably long.

4. NEWTON-KANTORIVITCH METHOD

The Newton-Kantorivitch method [31, 32] has also been applied to solve the above inverse problem.

Take variation on Eqs. (5) and (6) with respect to $J_j(\theta')$, A_{in} and B_{in}, one obtains

$$\begin{aligned}\delta E^{inc}(\mathbf{r}) = \sum_{j=1}^{2} \frac{\omega\mu_0}{4} \int_0^{2\pi} &\Big[J_j(\theta')\delta H_0^{(2)}(k_0 R_{ij}) \\ &+ H_0^{(2)}(k_0 R_{ij})\delta J_j(\theta')\Big]\, d\theta' \end{aligned} \tag{10}$$

$$\begin{aligned}\delta E^{scat}(\mathbf{r}) = \sum_{j=1}^{2} -\frac{\omega\mu_0}{4} \int_0^{2\pi} &\Big[J_j(\theta')\delta H_0^{(2)}(k_0 R_{j}) \\ &+ H_0^{(2)}(k_0 R_{j})\delta J_j(\theta')\Big]\, d\theta' \end{aligned} \tag{11}$$

where

$$\begin{aligned}
\delta E^{inc}(\mathbf{r}) &= -jk_0\cos(\theta-\varphi)E^{inc}(\mathbf{r})\delta F_i(\theta) \qquad \mathbf{r}\in C_i \\
\delta H_0^{(2)}(k_0R_{ii}) &= -\frac{k_0}{R_{ii}}H_1^{(2)}(k_0R_{ii})\cdot\Big\{\big[F_i(\theta)-F_i(\theta')\cos(\theta-\theta')\big]\delta F_i(\theta) \\
&\quad + \big[F_i(\theta')-F_i(\theta)\cos(\theta-\theta')\big]\delta F_i(\theta')\Big\} \\
\delta H_0^{(2)}(k_0R_{ij}) &= -\frac{k_0}{R_{ij}}H_1^{(2)}(k_0R_{ij})\cdot\{[F_i(\theta)\pm d\cos(\theta-\psi)]\,\delta F_i(\theta) \\
&\quad + \big[F_j(\theta')\mp d\cos(\theta'-\psi)\big]\delta F_j(\theta')\} \quad i\neq j \\
\delta H_0^{(2)}(k_0R_{j}) &= -\frac{k_0}{R_{j}}H_1^{(2)}(k_0R_{j})\cdot\big[F_j(\theta')\pm d_j\cos(\psi-\theta') \\
&\quad - R^{meas}\cos(\theta-\theta')\big]\,\delta F_j(\theta')
\end{aligned}$$

$$\delta F_j(\theta) = \sum_{n=0}^{N/2} \cos(n\theta)\delta A_{jn} + \sum_{n=1}^{N/2} \sin(n\theta)\delta B_{jn}$$
$$\delta F_j(\theta') = \sum_{n=0}^{N/2} \cos(n\theta')\delta A_{jn} + \sum_{n=1}^{N/2} \sin(n\theta')\delta B_{jn}$$

By applying the point-matching method with pulse basis function and Dirac delta test function on Eqs. (8) and (9), one gets

$$0 = \mathbf{L}_{11} \cdot \delta\mathbf{J} + \mathbf{L}_{12} \cdot \delta\mathbf{x} \tag{12}$$
$$\delta\mathbf{E}^{scat} = \mathbf{L}_{21} \cdot \delta\mathbf{J} + \mathbf{L}_{22} \cdot \delta\mathbf{x} \tag{13}$$

where

$$\delta\mathbf{J} = [\delta\mathbf{J}_1 \quad \delta\mathbf{J}_2]^T$$

The inversion equation is therefore obtained

$$\begin{aligned}\delta\mathbf{E}^{scat} &= \left(\mathbf{L}_{22} - \mathbf{L}_{21} \cdot \mathbf{L}_{11}^{-1} \cdot \mathbf{L}_{12}\right) \delta\mathbf{x} \\ &\triangleq \mathbf{M} \cdot \delta\mathbf{x}\end{aligned} \tag{14}$$

Finally, one gets the differential increment $\delta\mathbf{x}^n$ in the nth iteration in regularized form for multi-incidence case

$$\begin{aligned}\delta\mathbf{x}^n = &\left[\gamma\mathbf{R}^+ \cdot \mathbf{R} + \sum_{j=1}^{N_f \times N_a \times N_r} (\mathbf{M}_j^n)^+ \cdot \mathbf{M}_j^n\right]^{-1} \\ &\cdot \left[\sum_{j=1}^{N_f \times N_a \times N_r} (\mathbf{M}_j^n)^+ \cdot \delta\mathbf{E}_j^{scat}\right]\end{aligned} \tag{15}$$

where $\mathbf{R}$ is the regularization matrix and γ is the regularization factor.

Consequently, the shape functions are updated according to

$$\mathbf{x}^{n+1} = \mathbf{x}^n + \delta\mathbf{x}^n \tag{16}$$

The flow chart of NKM for microwave imaging of two parallel perfectly conducting cylinders is depicted in Fig. 3. The searching process starts from an initial guess $\mathbf{x}^0$, then goes into iterations updating the shape functions by Eq. (16). The NKM-type termination conditions are:

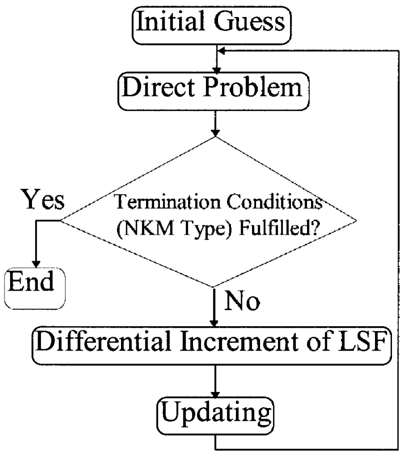

Figure 3. Flow chart of NKM for microwave imaging of two parallel perfectly conducting cylinders.

(1) $f^n(\mathbf{x}^n) < \varepsilon$
(2) $f^n(\mathbf{x}^n) > f^{n-1}(\mathbf{x}^{n-1})$
(3) Maximum iterations are used up

The numerical results in [32] show that the NKM tends to converge fast with a good starting point $\mathbf{x}^0$ and an exact knowledge on the values of d_1, d_2 and Ψ. However, further study shows that it is strictly subjected to the starting point and the knowledge on the values of d_1, d_2 and Ψ. It is more prone to get stuck in the local minima or even diverge. A *priori* is crucial for ensuring the convergence of the algorithm. Unfortunately, such a *priori* is not always available or accurate enough.

5. RGA COUPLED WITH NKM

Obviously, RGA and NKM behave complementarily while applied to microwave imaging of parallel perfectly conducting cylinders. It is therefore expected to develop a novel algorithm which inherits the merits of both RGA and NKM. RGA coupled with NKM (RGA-NKM) is consequently proposed. NKM is hybridized with RGA to improve the performances of both NKM and RGA. The flow chart of RGA-NKM is depicted in Fig. 2. It begins from an initial population which are generated randomly within the search space. Then, the algorithm enters into evolution loop searching for the optimum solution. In each evolution, a Newton-Kantorivitch type search for the local optimum is performed after the genetic evolution. The RGA provides the starting point of NKM. The best creature obtained by RGA after genetic evolution is used as the starting point of NKM. NKM is used to refine RGA to improve the local search ability of RGA.

6. NUMERICAL RESULTS

The RGA-NKM is used to reconstruct the first example in [49], two circular perfectly conducting cylinders with radius 0.3 m located on the x axis. $d_1 = d_2 = 0.5\text{m}$, $\psi = 0^\circ$. All the parameters are identical with those in [49] except stated otherwise. $\varepsilon = 1\%$.

Pseudo random noise is added into the scattered electric field data to investigate the effect of noise on the reconstructed result. The noise is assumed to be additive white noise with zero mean value.

To show the effect of noise quantitatively, a relative error of shape function between the reconstructed profile and the true one is defined as

$$DISC = \left\{ \frac{1.0}{2M} \sum_{i=1}^{2} \sum_{m=1}^{M} \frac{\left[\rho_{im}^{imag} - \rho_{im}^{true}\right]^2}{\rho^{2}{}_{im}^{true}} \right\}^{1/2} \tag{17}$$

where the superscript image and true stand for the reconstructed profile and the true one respectively

$$\rho_{im} = \left\{ [F_i(\theta_m)\cos\theta_m \pm d_i \cos\psi]^2 + [F_i(\theta_m)\sin\theta_m \pm d_i \sin\psi]^2 \right\}^{1/2}$$
$$\theta_m = \frac{2\pi}{M} m$$

To ensure that the proposed algorithm is practically useful, a false assumption is made on the values of d_1, d_2 and Ψ. To facilitate the comparison with RGA, they are set to be identical with those of example 4 in [49].

The inversion is performed on an IBM P-133 PC. It takes 64 minutes and 58 seconds to get the final results for the noise-free case as shown in Fig. 4. Seven generations of genetic evolution and 8 Newton-Kantorivitch type iterations are performed. It was demonstrated in [49] that the it took the RGA 393 generations of genetic evolution to get the final result.

The effect of random noise is shown in Figs. 5 and 6. It can be seen that the reconstructed results with signal-to-noise ratio 14 dB or

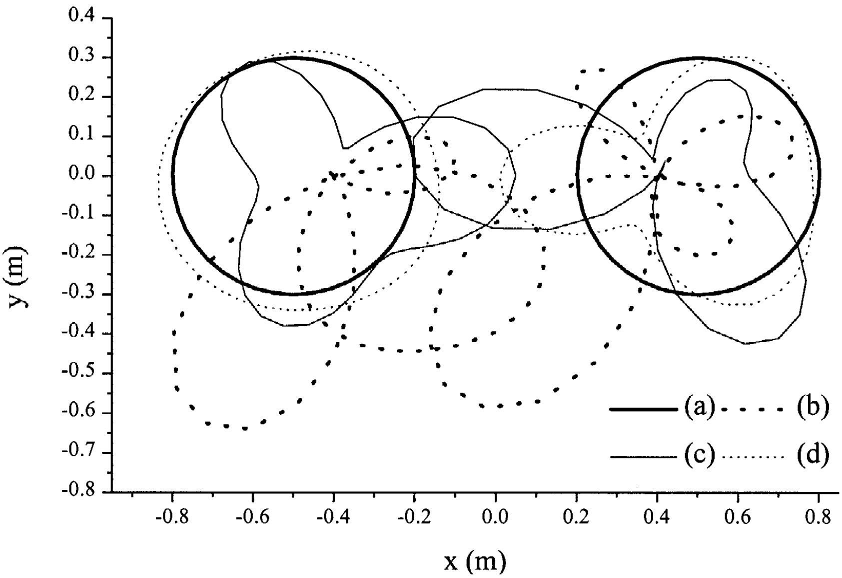

Figure 4. Inversion results of example 1 with noise-free data (a) true profile (b) initial guess (c) starting point for NKM and (d) inversion result after one Newton-Kantorivitch iteration. The final result is exactly the same as the true profile.

higher is very accurate. Fig. 5 also shows the effect of random noise on RGA for reconstructing this example. The typical inversion results by RGA using random noise contaminated data are shown in Fig. 7. To speed up the inversion process, the values of d_1, d_2 and Ψ for this case are assumed to be known exactly in advance. This may improve the noise-tolerance level of RGA.

Obviously, the RGA converges much more slowly than the RGA-NKM. In addition, Fig. 5–7 demonstrate that the noise-tolerance level of RGA-NKM is improved slightly.

The NKM is also used to invert the above object. The values of d_1, d_2 and Ψ for this case are assumed to be known exactly in advance. Four cases are considered:

Case 1: Generate the initial guess randomly within the same search range. Twenty trials were simulated. In our simulation, none of the trials succeeds

Case 2: Set the initial guess of the coefficients as their mean values of

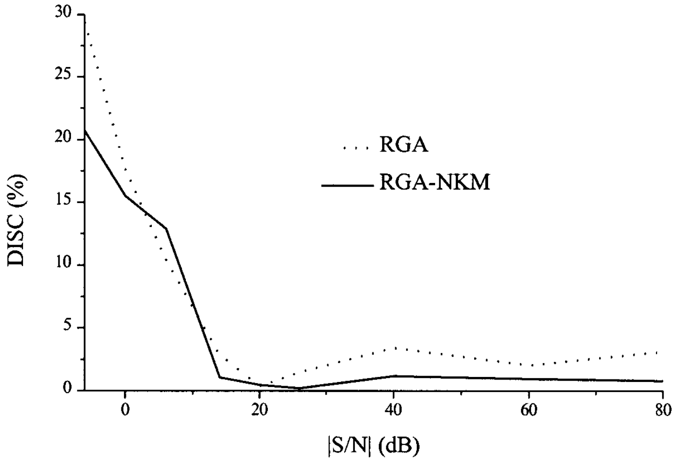

Figure 5. Effect of noise.

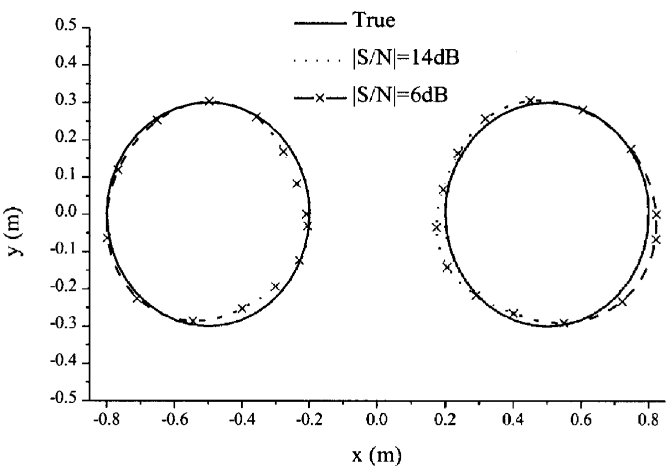

Figure 6. Inversion results of example 1 by RGA-NKM with noisy data.

the search range, i.e., $A_{i0} = 1.0,\ (A_{ij}, B_{ij}) = 0,\ i = 1 \sim 2,\ j = 1 \sim 4$. The NKM fails.

Case 3: Set the initial guess as the two extreme cases of the search range, i.e., (i) $A_{i0} = 0,\ (A_{ij},\ B_{ij}) = -0.5,\ i = 1 \sim 2,\ j = 1 \sim 4$ (ii)

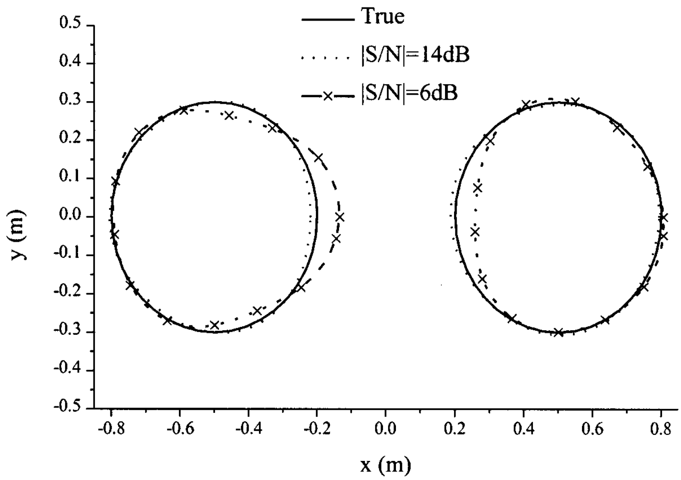

Figure 7. Inversion results of example 1 by RGA with noisy data.

$A_{i0} = 2$, $(A_{ij},\ B_{ij}) = 0.5$, $i = 1 \sim 2$, $j = 1 \sim 4$. The NKM fails for both of them.

Case 4: Set the initial guess to be identical with that of the RGA-NKM which is the best one among the initial population. The NKM fails.

Comparing the simulation results by RGA-NKM with those by NKM, it is found that the RGA-NKM shows a much higher level of robustness than NKM.

The RGA-NKM is used to reconstruct the second and third example in [49] too. The measured(simulated) scattering data here are assumed to be noise-free. The inversion results are shown in Figs. 8 and 9. The inversion takes 50 minutes 45 seconds and 19 minutes 18 seconds respectively.

7. CONCLUSIONS

In this paper, NKM is hybridized with RGA to improve the performance of both RGA and NKM. A novel inversion algorithm, RGA-NKM, for microwave imaging of perfectly conducting cylinders with or without the effect of random noise is proposed. The main idea of the RGA-NKM is to perform a Newton-Kantorivitch type search for the local optimum after the genetic operations in each genetic

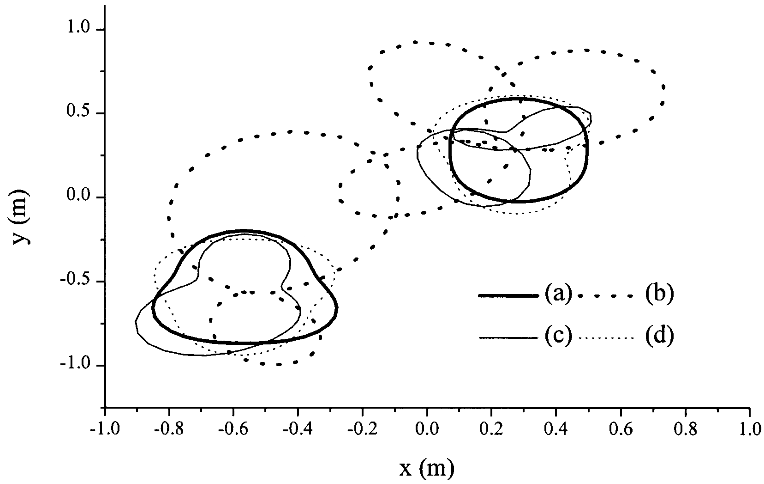

Figure 8. Inversion results of example 2 with noise-free data (a) true profile (b) initial guess (c) starting point for NKM and (d) inversion result after one Newton-Kantorivitch iteration. The final result is exactly the same as the true profile.

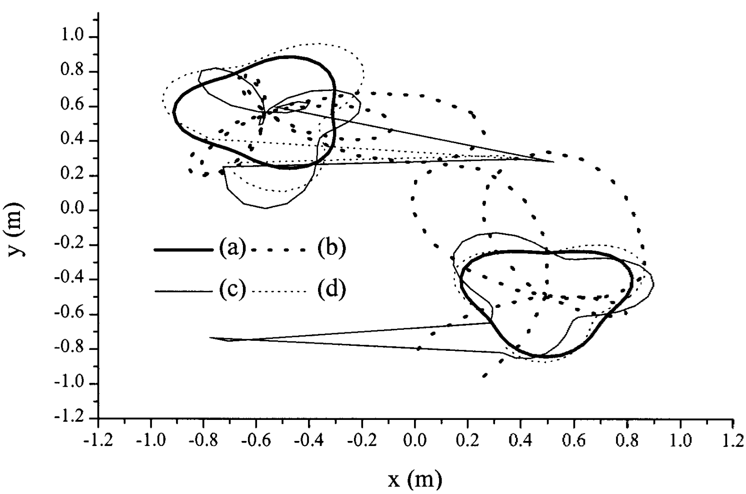

Figure 9. Inversion results of example 3 with noise-free data (a) true profile (b) initial guess (c) starting point for NKM and (d) inversion result after one Newton-Kantorivitch iteration. The final result is exactly the same as the true profile.

evolution. The RGA provides the starting point of NKM. The best creature obtained by RGA after genetic evolution acts as the starting point of NKM. The NKM refines RGA to improve the local search ability of RGA.

Numerical results and comparisons with both RGA and NKM demonstrate that the RGA-NKM retains the advantages of RGA such as high level of robustness, versatility and insensitiveness to ill-posedness, greatly improves the search ability and speeds up the convergence.

On the other hand, the RGA-NKM is not without drawbacks. It loses its simplicity since the NKM is hybridized.

REFERENCES

1. Tijhuis, A. J., *Electromagnetic Inverse Profiling: Theory and Numerical Implementation,* VNU Science Press, Utrecht, The Netherlands, 1987.
2. Chew, W. C., *Waves and Fields in Inhomogeneous Media,* van Nostrand Reinhold, New York, 1990.
3. Qing, A., "Electromagnetic scattering and inverse scattering," Ph.D. Dissertation, Southwest Jiaotiong University, Chengdu, May 1997.
4. Colton, D. and R. Kress, *Inverse Acoustic and Electromagnetic Scattering Theory,* 2nd ed., Springer-Verlag, New York, 1998.
5. Chen, L. C., et al., "Improved performance of a subsurface radar target identification system through antenna design," *IEEE Trans. Antennas Propagat.,* AP-29, 307–311, 1981.
6. Bolomey, J. C., et al., "Microwave diffraction tomography for biomedical applications," *IEEE Trans. Micro. Theory Tech.,* MTT-30, 1998–2000, 1982.
7. Pichot, C. and L. Chommeloux, "Algorithms for active microwave imaging-biomedical and civil engineering applications," *Proc. US-France Conf. On Near Field Microwave Imaging,* Atlanta, 1985.
8. Farhat, H. H., "Microwave diversity imaging and automated target identification based on models of neural networks," *Proc. IEEE,* 77, 670–681, 1989.
9. Wang, Y. M. and W. C. Chew, "Limited angle inverse scattering problems and their applications for geophysical explorations," *Int. J. Imaging Systems Tech.,* 2(2), 96–111, 1990.
10. Louis, A. K., "Medical imaging: state of the art and future development," *Inverse Problems,* 8, 709–738, 1992.

11. Liu, Q. H., "Nonlinear inversion of electrode-type resistivity measurements," *IEEE Trans. Geosci. Remote Sens.,* GE-32(3), 499–507, 1994.
12. Meaney, P. M., K. D. Pausen, and J. T. Chang, "Near-field microwave imaging of biologically-based materials using a monopole transceiver system," *IEEE Trans. Micro. Theory Tech.,* MTT-46(1), 31–45, 1998.
13. Golden, K. M., et al., "Inverse electromagnetic scattering models for sea ice," *IEEE Trans. Geosci. Remote Sens.,* GE-36(5), 1675–1704, 1998.
14. Bube, K. P. and R. Burridge, "The one-dimensional inverse problem of reflection seismology," *SIAM Rev.,* 25(4), 497–559, 1983.
15. Devancy, A. J., "Nonuniqueness in the inverse scattering problem," *J. Math. Phys.,* 19(7), 1526–1531, 1978.
16. Sarkar, T. K., D. D. Weiner, and V. K. Jain, "Some mathematical considerations in dealing with the inverse problems," *IEEE Trans. Antennas Propagat.,* AP-29, 373–379, 1981.
17. HoLmann, B. and O. Scherzer, "Factors influencing the ill-posedness of nonlinear problems," *Inverse Problems,* 10, 1277–1297, 1994.
18. Habashy, T. M. and R. Mittra, "On some inverse methods in electromagnetics," *J. Electromag. Waves Appli,* 1(1), 25–58, 1987.
19. Lewis, R. M., "Physical optics inverse diffraction," *IEEE Trans. Antennas Propagat.,* AP-17, 308–314, 1969.
20. Bojarski, N. N., "A survey of the physical optics inverse scattering identity," *IEEE Trans. Antennas Propagat.,* AP-30, 980–989, 1982.
21. Slaney, M., A. C. Kak, and L. E. Larsen, "Limitations of imaging with first-order diffraction tomography," *IEEE Trans. Micro. Theory Tech.,* MTT-32(8), 860–874, 1984.
22. Sezginer, A., "Forward and inverse problems in transient electromagnetic fields," Ph.D. Dissertation, M.I.T., 1985.
23. Burridge, R., "The Gel'fand-Levitan, the Marchenko, and the Gopinath-Sondhi integral equation of inverse scattering theory, regarded in the context of inverse impulse-response problems," *Waves Motion,* 2, 305–323, 1980.
24. Balanis, G. N., "The plasma inverse problem," *J. Math. Phys.,* 13, 1001–1005, 1972.
25. Habashy, T. M., "A generalized Gel'fand-Levitan-Marchenko integral equation," *Inverse Problems,* 7, 703–711, 1991.
26. Keller, J. B., "Accuracy and validity of Born and Rytov approximations," *J. Opt. Soc. Am.,* 59, 1003–1004, 1969.

27. Moghaddam, M. and W. C. Chew, “Nonlinear two-dimensional velocity profile inversion using time-domain data,” *IEEE Trans. Geosci. Remote Sens.,* GE-30(1), 147–156, 1992.
28. Qing, A. and L. Jen, “Microwave imaging of dielectric cylinder in layered media,” *J. Electromag. Waves Appli.,* 11(2), 259–269, 1997.
29. Chew, W. C. and Q. H. Liu, “Inversion of induction tool measurements using the distorted Born iterative method and CG-FFHT,” *IEEE Trans. Geosci. Remote Sens.,* GE-32(4), 878–884, 1994.
30. Chew, W. C. and Y. M. Wang, “Reconstruction of two-dimensional permittivity using the distorted Born iterative method,” *IEEE Trans. Medical Imaging,* MI-9, 218–225, 1990.
31. Roger, A., “Newton-Kantorivitch algorithm applied to electromagnetic inverse problem,” *IEEE Trans. Antennas Propagat.,* AP-29, 232–238, 1981.
32. Chiu, C. C. and W. W. Kiang, “Microwave imaging of multiple conducting cylinders,” *IEEE Trans. Antennas Propagat.,* AP-40, 933–941, 1992.
33. Qing, A. and L. Jen, “A novel method for microwave imaging of dielectric cylinder in layered media,” *J. Electromag. Waves Appli.,* 11(1), 1337–1348, 1997.
34. Colton, D. and P. Monk, “A novel method for solving the inverse scattering problem for time-harmonic acoustic waves in the resonance region,” *SIAM J. Appl. Math.,* 45, 1039–1053, 1985.
35. Colton, D. and P. Monk, “A novel method for solving the inverse scattering problem for time-harmonic acoustic waves in the resonance region II,” *SIAM J. Appl. Math.,* 46, 506–523, 1986.
36. Hettlich, F., “Two methods for solving an inverse conductive scattering problem,” *Inverse Problems,* 10, 375–385, 1994.
37. Chew, W. C. and G. P. Otto, “Microwave imaging of multiple conducting cylinders using local shape functions,” *IEEE Micro. Guided Wave Lett.,* 2(7), 284–286, 1992.
38. Weedon, W. H. and W. C. Chew, “Time-domain inverse scattering using the local shape function method,” *Inverse Problems,* 9, 551–564, 1993.
39. Otto, G. P. and W. C. Chew, “Inverse scattering of Hz waves using local shape-function imaging: a T-matrix formulation,” *Int. J. Imaging Systems Tech.,* 5(1), 22–27, 1994.
40. Otto, G. P. and W. C. Chew, “Microwave inverse scattering-local shape function imaging for improved resolution of strong scatterers,” *IEEE Trans. Micro. Theory Tech.,* MTT-42(1), 137–141, 1994.

41. Kleinman, R. E. and P. M. van den Berg, "A modified gradient method for two-dimensional problems in tomography," *J. Comput. Appl. Math.,* 42(1), 17–35, 1992.
42. Kleinman, R. E. and P. M. van den Berg, "An extended range-modified technique for profile inversion," *Radio Sci.,* 28, 877–884, 1993.
43. van den Berg, P. M. and M. van der Horst, "Nonlinear inversion in induction logging using the modified gradient method," *Radio Sci.,* 30, 1355–1369, 1995.
44. Ney, M. M., A. M. Smith, and S. Studchly, "A solution of electromagnetic imaging using pseudoinverse transformation," *IEEE Trans. Med. Imaging,* MI-3, 155–162, 1984.
45. Tarantola, A. and B. Valette, "Generalized nonlinear inverse problems solved using the least squares criterion," *Rev. Geophy. Space Phy.,* 20, 219–232, 1982.
46. Tarantala, A., *Inverse Problem Theory,* Elsevire Science, New York, 1987.
47. Chiu, C. C. and P. T. Liu, "Image reconstruction of a perfectly conducting cylinder by the genetic algorithm," *IEE Proc. Microw., Antennas Propagat.,* 143(3), 249–253, 1996.
48. Qing, A. and C. K. Lee, "Shape reconstruction of a perfectly conducting cylinder using real-coded genetic algorithm," *Dig. 1999 IEEE AP-S and URSI Symp.,* 2148–2151, Orlando, 1999.
49. Qing, A., C. K. Lee, and L. Jen, "Microwave imaging of parallel perfectly conducting cylinders using real-coded genetic algorithm," *J. Electromag. Waves Appli.,* 13(8), 1121–1143, 1999.
50. Qing, A. and S. Zhong, "Microwave imaging of two-dimensional perfectly conducting objects using real-coded genetic algorithm," *Dig 1998 IEEE AP-S and URSI Symp.,* Atlanta, 726–729, 1998.
51. Xiao, F. and H. Yabe, "Microwave imaging of perfectly conducting cylinders from real data by micro genetic algorithm couple with deterministic method," *IEICE trans. Electron.,* E81-C(12), 1784–1792, 1998.
52. Meng, Z. Q., T. Takenaka, and T. Tanaka, "Image reconstruction of two-dimensional impenetrable objects using genetic algorithm," *J. Electromag. Waves Appli.,* 13(1), 95–118, 1999.
53. Holland, J. H., *Adaptation in Natural and Artificial Systems,* Michigan Univ., Ann Arbot, Michigan, 1975.
54. Davis, L., *Genetic Algorithm and Simulated Annealing,* Pittman, London, 1987.
55. Goldberg, D. E., *Genetic Algorithms in Search, Optimization and Machine Learning,* Addison-Weiley, Reading, MA, 1989.

56. Chen, G. L., X. F. Wang, Z. Q. Zhuang, and D. S. Wang, *The Genetic Algorithms and Applications,* People's Telecommunication Press, Beijing, 1996. (in Chinese)
57. Michielssen, E., S. Ranjithan, and R. Mittra, "Optimal multilayer filter design using real coded genetic algorithm," *IEE Proc. J,* 139(6), 413–420, 1992.
58. Haupt, R., "Comparison between genetic and gradient-based optimization algorithms for solving electromagnetics problems," *IEEE Trans. Magn.,* 31(3), 1932–1935, 1995.
59. Haupt, R. L., "An introduction to genetic algorithms for electromagnetics," *IEEE Antennas Propagat. Mag.,* 37(2), 8–15, 1995.
60. Weili, D. S. and E. Michiessen, "Genetic algorithm optimization applied to electromagnetics: a review," *IEEE Trans. Antennas Propagat.,* AP-45(3), 343–353, 1997.
61. Yeo, B. K. and Y. Lu, "Array failure correction with a genetic algorithm," *IEEE Trans. Antennas Propagat.,* AP-47(5), 823–828, 1999.
62. Harrington, R. F., *Field Computation by Moment Methods,* IEEE Press, New York, 1993.